Designing structured surfaces that repel fluid-borne particles

Carina Semmler and Alexander Alexeev

Phys. Rev. E **84**, 066303 — Published 5 December 2011

DOI: 10.1103/PhysRevE.84.066303

Designing structured surfaces that repel fluid-borne particles

Carina Semmler
Institute of Fluid Mechanics
Karlsruhe Institute of Technology, Karlsruhe, Germany, D-76131

Alexander Alexeev*
George W. Woodruff School of Mechanical Engineering
Georgia Institute of Technology, Atlanta, GA 30332

Abstract

Using computational modeling, we examine particle-laden flows along surfaces decorated with periodic arrays of tilted posts. We show that when high-aspect-ratio posts are tilted against the flow direction, cross-stream circulatory secondary flows emerge. These circulatory flows enhance the net lift force acting on finite-sized particles transported by fluid, thereby repelling the particles from the wall and preventing their deposition. This hydrodynamic effect can be potentially used for designing antifouling and self-cleaning surfaces.

* Corresponding author: alexander.alexeev@me.gatech.edu

Introduction

In many industrial applications, fouling and deposition of particles on surfaces are factors that can greatly impair the efficiency. For example in microfluidic devices in which different synthetic and biological particles are transported by a fluid flow for processing and analysis, the attachment of particles to internal surfaces can hinder and potentially block the flow, thereby precluding the normal device operation [1-3]. It is, therefore, important to develop surfaces that can effectively prevent the formation of surface deposits or self-clean and, in this manner, can ensure reliable device operation.

Similarly, formation of bacterial biofilms on fluid-exposed surfaces is a critical issue in biomedical applications, food processing, and water purification technology. Marine bio-fouling causes decreased efficiency of heat exchangers, sensors, and ship propulsion and, therefore, requires effective methods for fouling control [4-8]. For example, the formation of a 10μm biofilm on a ship hull results in a 1% increase in fuel consumption [5].

Current methods for fouling mitigation harness electrical and magnetic fields that physically repel fouling particles from surfaces [9-10]. In this scenario, however, bulky and sophisticated equipment is typically needed, which increases overall cost and requires additional operational power. Furthermore, specific requirements to particle material properties may be imposed by these methods. Thermophoretic effects were also used to prevent contamination of heated surfaces [10]. Hydrodynamic microstreaming flows associated with acoustic waves or periodically beating synthetic cilia can reject fluid suspended particles away from the walls and, therefore, could be potentially employed in fouling control [11-13]. Additionally, different electrochemical methods and

chemical compounds employing antibiologic agents toxic to microorganisms were developed to prevent biofilm formation and growth [6-7]. These chemical methods are especially attractive for marine applications, but can degrade with time and can be potentially harmful for the environment.

Herein, we use computer simulations to examine the design of structured surfaces that can prevent deposition of microscopic solid particles transported by flowing fluid. We have recently shown that surfaces covered with bio-mimetic synthetic cilia can effectively attract solid neutrally-buoyant particles propelled in a pressure-driven channel flow by inducing cross-stream particle drift towards ciliated walls [14-15]. In this microfluidic system, elastic filaments attached to a channel wall are deflected by the flowing fluid and create secondary streams that direct suspended particles toward the solid wall. It was found that the magnitude of the secondary flows is set by the cilium deflection, which in turn is defined by the cilium elasticity.

We have also demonstrated that surfaces decorated with nanoscopic rigid posts can regulate spatial distribution of diffusive nanoparticles and linear macromolecules transported by a shearing flow [15-16]. Specifically, nanoposts tilted along the flow hydrodynamically attract the suspended solutes, whereas nanoposts tilted against the flow create a repulsive effect and prevent the deposition of nanoparticles even if the posted surface is adhesive. Furthermore, it was found that the repulsive effect is different for chains and nanoparticles allowing separation of colloid-polymer mixtures.

Here, we probe how this concept can be harnessed for designing passive antifouling surfaces that hydrodynamically repel particles suspended in a fluid flow. Our goal is to evaluate the magnitude of the hydrodynamic repelling force that can be crated

by tilted posts and to examine how this force depends on the relative particle size and tilt angle. To this end, we consider a shear-driven flow along a substrate decorated with a periodic array of rigid, high-aspect-ratio posts tilted against the flow direction. We introduce micrometer-seized non-Brownian solid particles which are comparable in size with the inter-post separation. We apply an external body force to the particles directed towards the posted surface (e.g. gravity) to assess the magnitude of the hydrodynamic repelling forces created by the surface structures. Our simulations reveal that, depending on particle size, posted walls can increase the hydrodynamic lift by an order of magnitude compared to channels with smooth walls.

Methodology

We model channel flow along a posted wall using a lattice-Boltzmann model (LBM) for the hydrodynamics of viscous fluids [17]. LBM is a lattice-based method for simulating fluid flows governed by the Navier-Stokes equations. We use a three-dimensional model with 19 velocities (D3Q19) [18]. In this model, a velocity distribution function $f_i(\mathbf{r},t) \equiv f(\mathbf{r},\mathbf{c}_i,t)$ describes the mass density of fluid particles with velocity $\mathbf{c}_i$ in a lattice node $\mathbf{r}$ at time t. The hydrodynamic quantities are moments of the distribution function, i.e., the mass density $\rho = \sum_i f_i$, the momentum density $\mathbf{j} = \rho\mathbf{u} = \sum_i \mathbf{c}_i f_i$ with $\mathbf{u}$ being the local fluid velocity, and the momentum flux $\Pi = \sum_i \mathbf{c}_i \mathbf{c}_i f_i$. Hereafter, all dimensional values are given in lattice Boltzmann units (lbu).

The time evolution of the distribution function is governed by the discretized Boltzmann equation $f_i(\mathbf{r}+\mathbf{c}_i\Delta t, t+\Delta t) = f_i(\mathbf{r},t) + \Omega[\mathbf{f}(\mathbf{r},t)]$, where Ω represents the collision operator that accounts for the change in f_i due to instantaneous collisions at the lattice nodes. Here, $\mathbf{f}(\mathbf{r},t)$ denotes all the distributions f_i in a node $\mathbf{r}$ at time t. We use a multi-relaxation time collision operator that conserves mass and momentum and relaxes the fluid stress toward local equilibrium [18].

To model rigid posts attached to the channel wall, we use immobile nodes arranged on a simple cubic lattice. The outer surfaces of this lattice define the post geometry and the solid-fluid interface. The solid particle is modeled as a fluid-filled rigid shell using an approach that is based on the lattice spring model (LSM) [19-20]. The spherical particle is constructed from two concentric layers of nodes that are uniformly distributed on capsule surface [21]. We set the particle solid density equal to the fluid density. We keep the relative distances between the nodes constant, thus the particle obeys the dynamics of rigid solid body. The particle translational and rotational dynamics is captured by integrating Newton's equation of motion for the shell nodes, $\mathbf{F}(\mathbf{r}_i) = m\left(d^2\mathbf{r}_i/dt^2\right)$, using the velocity Verlet algorithm. Here, $\mathbf{F}$ is the total force on the node $\mathbf{r}_i$ with mass m that includes the force exerted by the fluid at the solid-fluid interface [22-23].

To impose the no-slip boundary condition at the solid-fluid interface of the particle and posts, we employ an interpolation bounce-back rule that accounts for the actual interface position and velocity [24]. Specifically, the bounce-back rule is applied to the distributions that cross the surfaces of moving particle and static posts. In this implementation, solid particle and posts impose velocity on the nearby flow and

experience forces due to fluid stresses, thereby resulting in a fully-coupled fluid-structure simulation approach.

We have previously validated this hybrid computational method in the limit of small Reynolds numbers and applied it to study the motion of microscopic particles in microchannels [25-29]. The details of our computational method can be found elsewhere [21-23].

Computational setup

Our three-dimensional simulation domain has length L_x, height L_y, and width L_z (Fig. 1). The bottom of the channel is lined with regularly distributed rigid posts with length L and width b. The posts are arranged in a square pattern and are tilted relative to the flow direction with an angle α. In the x and z directions, we impose periodic boundary conditions. The channel is filled with a Newtonian fluid with the density $\rho = 1$ and the dynamic viscosity $\mu = 1/6$ (in lbu). The upper channel wall moves with a constant velocity of $V_{wall} = 0.01$, which sets the fluid in motion and creates a shear flow in the channel with a rate $\dot{\gamma} = V_{wall}/L_y$. The flow is characterized by the channel Reynolds number $\mathrm{Re} = V_{wall} L_y / \nu = 6$, where $\nu = \mu/\rho$ is the kinematic viscosity.

We set the post length $L = 40$, width $b = 0.1L$, and the distance between neighboring posts $B = L$. We introduce into the channel a spherical solid particle of radius R that can move freely inside the array of posts. We consider that the particle is sufficiently large and it is not affected by Brownian fluctuations. Moreover, we set

$L_x = 4.4L$, $L_y = 2.5L$, and $L_z = 3.3L$. Thus, the bottom channel wall encompasses an array of 4×3 tilted posts (Fig. 1).

We apply an external force F_E to the particle, which acts in the negative y direction. To characterize the magnitude of this force, we define a dimensionless force $W = F_E / F_L$, where F_L is the lift force on a particle moving in a shear flow in a channel with smooth walls. We estimate the latter force by $F_L = 6\pi\mu R V_L$, where $V_L \approx 3/32\, RU^2 \nu^{-1}$ is the velocity normal to the wall of a particle moving with a velocity U along a stationary wall [30]. We approximate $U \approx \dot{\gamma} R$, which results in $W = 16 F_E / 9\pi\rho R^4 \dot{\gamma}^2$.

Results and discussion

In a shear channel flow, particles migrate away from the walls and equilibrate at the channel center-line. This migration is driven by the wall effect due to an increased pressure in the gap between the particle and the nearby channel wall. Particles affected by an external force acting across the flow direction equilibrate closer to the wall at which the force is pointing and, when the force is strong enough, deposit on the surface of this wall. To examine the effect of surface microstructure on the particle motion and equilibration, we calculated trajectories of a particle in a channel with smooth walls and in a channel in which the bottom wall is decorated with tilted posts (Fig. 2). We apply to the particle an external force directed downwards, which is expressed in terms of the dimensionless parameter W.

In Fig. 2, the particle starts at height $y = 0.167L_y$ at which it equilibrates in a channel with smooth walls when the force is set to $W = 1.05$. Indeed, we find that the particle with this force moves parallel the channel axis in the smooth channel, which means that the external force is balanced by the hydrodynamic lift force. When we introduce a particle with the same external force $W = 1.05$ in a channel with surface posts, it follows an oscillatory trajectory that rapidly departs from the structured bottom wall. Furthermore, even when we increase the force six times, we find that the particle moves away from the bottom wall as it is propelled along the channel by the flow. This result indicates that tilted posts attached to the bottom channel wall enhance lift force acting on particles.

The lift force enhancement takes place due to cross-stream circulatory flows emerging in the layer of tilted posts. Figure 3 presents the averaged cross-stream flow velocity in channels with posts with different tilt angles. Here, we average flow velocity over one period of wall structure in the x direction. When the posts are oriented normal to the surface of the channel wall, no significant secondary flows appear within the layer of posts (Fig. 3a). When posts are tilted with respect to the flow direction, circulatory flows emerge near the posted wall. Specifically, when the posts are tilted against the flow direction, the fluid in the middle between post rows on average moves upwards, whereas the fluid closer to posts has the average velocity directed downwards (Fig. 3b).

The appearance of this fluid circulation in the layer of tilted posts is related to the difference in fluid drag between flows directed along and normal to the high-aspect-ratio rigid posts. Drag force is twice larger when the fluid flow is normal to a solid rod than in the case when the fluid flows along the rod [31]. Thus, when surface posts are tilted with

respect to the flow direction, the fluid tends to flow along the posts to minimize the energy loss. Specifically, when the posts are tilted against the flow, the fluid near posts flows along the posts and towards the bottom wall of the channel. Continuity requires that the fluid returns in the middle between two post rows creating an uprising flow and a flow circulation (Fig. 3b). Thus, when a solid particle is located in the gap between two rows of tilted posts, it experiences a hydrodynamic force due to this uprising flow that pushes the particle away from the solid wall, thereby enhancing the lift.

We note that when posts are tilted along the flow, the direction of flow circulation reverses and the fluid in the gap between post rows moves towards the posted wall, in which case particles suspended in the fluid migrate to towards this surface [14, 16]. Furthermore, when posts are attached normal to the channel wall, the flow near the post surface is nearly symmetrical relative to the channel axis. In this situation, no net flow circulation emerges and the posts oriented normal to the flow direction do not affect the trajectories of suspended particles [14, 16].

The force that fluid circulation imposes to the particle depends on particle position in the channel. When a particle is centered between two post rows the force is maximized. However, when a particle moves closer to one of the post rows, it is only partly affected by the fluid that moves upwards, thereby decreasing the lift force on the particle. In Fig. 4, we show the equilibrium positions of particles with $W = 8.37$ that are located at different positions relative to the surface posts. To find the equilibrium position, we average the particle trajectory for one period of particle motion in the x direction. Indeed, we find that in the middle between post rows the particle equilibrates farther from the wall due to a larger lift, whereas particles move closer to the bottom

when they are near posts where they experience a weaker lift force. We also find that when the particles are initially placed at a lateral distance from the posts that is somewhat smaller than the particle radius, the particles are rapidly deflected to a trajectory that avoids posts and is closer to the channel centerline. This occurs without direct collisions with the posts and is facilitated by a repulsive hydrodynamic force that arises between stationary rigid posts and the moving particle transported by the flow.

It is constructive to estimate the maximum external force on a particle that can be balanced by the enhanced lift on posted surfaces. To this end, we introduce particles close to the posts where the lift force is minimum and track their motion in the channel subject to different external forces. Figure 5 shows typical trajectories in the cross-stream $y-z$ plane corresponding to particles with different W. In all the cases presented in this figure particles start at $y=0.16L_y$ and $z=-0.25B$. The particles follow oscillatory trajectories and slowly migrate to the middle of the gap between post rows and downwards driven by the combination of an external force and a drag force due to the circulatory flow in the channel. When the external force is large enough, the particle reaches the bottom wall and deposits on the solid surface. For weaker external forces, the particle first moves downwards, but when it approaches the upwards stream of the vortex due to its motion to the channel centerline, the lift increases and the particle starts moving upwards before it touches the bottom wall. We, therefore, can identify the critical force as the largest external force at which a particle exhibits the upward motion.

While this approach may give a relatively accurate estimate of the critical force, it requires long time simulations, since the magnitude of flow velocity near the channel wall is small and particles propel very slowly. To reduce the simulation time, we

introduce particles positioned in such a way that the gap between a particle and channel surface is equal to 1 lbu. This distance is sufficiently large to resolve hydrodynamic interactions between the particle and channel wall [18]. In the z direction, we also set an initial gap of 1 lbu between the particle surface and the posts. We then systematically vary the external force W and measure the period averaged vertical velocity of particle motion after the initial transient. We define the critical force W_{cr} as the force for which the vertical velocity is nil, i.e. the particle on average moves parallel to the wall.

The critical force W_{cr} found from these simulations is shown in Fig. 6 as a function of particle size. We also show in this figure the critical force in channels with smooth walls which is found to be equal to approximately unity. The simulations show that W_{cr} in posted channels increases with decreasing particle radius and for all particle sizes it exceeds W_{cr} in smooth channels (see inset in Fig. 6). We note that the dimensionless force W is proportional to $F_E R^4$, which means that the dimensional critical force F_{Ecr} increases with particle radius.

We also note that the critical force for particles that are initially placed close to a posted surface is somewhat lower than that found by analyzing trajectories of particles that start at a certain distance above the surface. This is due to a weaker uprising flow in the vicinity of posts compared to that closer to the channel mid-plane towards which the particles drift when they move downwards (Fig. 5). Specifically, for particles shown in Fig. 5 we found that the critical force is about 40% greater than that found in the calculations shown in Fig. 6.

We can compare the critical force on particle F_{Ecr} with particle weight $V_p \rho_s g$ and buoyancy force $V_p \rho g$ in order to estimate the minimum shear rate $\dot{\gamma}_{cr}$ that is required to keep particle in flow. Here, $V_p = 4/3\pi R^3$ is the particle volume, ρ_s is the solid density, and g is gravitational acceleration. From the condition $F_{Ecr} > 4/3\pi R^3(\rho_s - \rho)g$, we find $\dot{\gamma}_{cr} = 8/3\sqrt{g(\rho_s - \rho)/(3W_{cr}\rho R)}$. For biological cells with the radius $R \approx 10^{-5}\,\mathrm{m}$ and density $\rho_s \approx 1.1\,\mathrm{g/mL}$ [32] in water solution with $\rho \approx 1\,\mathrm{g/mL}$ and by setting $W_{cr} \approx 10$, we find $\dot{\gamma}_{cr} \approx 150\,\mathrm{s}^{-1}$ which is in the range of experimentally realistic values [2].

Finally, we probed how the lift enhancement depends on the tilt angle of surface posts. When the posts are oriented along or normal to the surface, no secondary flows emerge in the channel, whereas for intermediate values of the post angle, the flow vorticity is maximized. Figure 7 shows how the equilibrium position of a particle with $R = 0.25L$ varies with the post tilt. We find that the equilibrium position exhibit a maximum at $\alpha = 40°$. It means this angle leads to the most intensive flow circulation and, therefore, is optimal for enhancing lift on suspended particles.

Summary

Using three-dimensional computer simulations, we design a patterned surface that can hydrodynamically repel solid particles transported by a viscous fluid. The surface encompasses a regular array of thin rigid posts that are arranged in a square pattern and tilted against the flow direction. The posts create circulating secondary flows that confront particle deposition on the posted surface. We examined the motion of different-

sized non-Brownian particles in a low-Reynolds-number shear flow along this patterned surface and evaluated the magnitude of lift force acting on these particles. We found that the hydrodynamic lift on particles is significantly enhanced due to tilted surface posts compared to a similar flow in channels with smooth walls. We also found that the secondary flows and, consequently, the lift force are maximized when the posts are tilted to an angle of $40°$ relative to the channel surface.

In microfluidic applications, adhesive forces may play a major role in surface fouling. In our current work targeted to evaluate the magnitude of the hydrodynamic lift induced by structured surface, we did not considered attractive interactions between particles and channel surfaces. Nonetheless, our results may be useful to estimate the effect of posts on the fouling of adhesive surfaces. In this situation, the critical force should be compared to the magnitude of a characteristic force of the adhesive interaction between particles and surface.

Since such posted surfaces can be fabricated using modern manufacturing techniques [33-38], our findings open a new way for designing anti-fouling surfaces that can effectively repel various synthetic and biological microparticles using hydrodynamic forces arising in a flowing fluid, thereby reducing the deposition and surface fouling. The action of these anti-fouling surfaces is independent of specific chemical or material properties of particulates, which makes the method potentially useful in a broad range of engineering applications including filtering, water remediation, particle separation, cell enrichment, and as anti-bacterial and self-cleaning coatings.

Acknowledgment

Partial financial support from NSF under Award No. 0932510 is gratefully acknowledged.

References

[1] T.M. Squires, S.R. Quake, Rev Mod Phys, 77 (2005) 977-1026.
[2] H.A. Stone, A.D. Stroock, A. Ajdari, Annu. Rev. Fluid Mech., 36 (2004) 381-411.
[3] D.A. Ateya, J.S. Erickson, P.B. Howell, L.R. Hilliard, J.P. Golden, F.S. Ligler, Anal Bioanal Chem, 391 (2008) 1485-1498.
[4] H.C. Flemming, Appl Microbiol Biot, 59 (2002) 629-640.
[5] J.J. Cooney, Helgolander Meeresun, 49 (1995) 663-677.
[6] A. Whelan, F. Regan, J Environ Monitor, 8 (2006) 880-886.
[7] D.M. Yebra, S. Kiil, K. Dam-Johansen, Prog Org Coat, 50 (2004) 75-104.
[8] N. Dror, M. Mandel, Z. Hazan, G. Lavie, Sensors-Basel, 9 (2009) 2538-2554.
[9] C.I. Calle, C.R. Buhler, J.L. McFall, S.J. Snyder, J Electrostat, 67 (2009) 89-92.
[10] R. Kohli, K.L. Mittal, Developments in surface contamination and cleaning: fundamentals and applied aspects, W. Andrew Pub., Norwich, NY, U.S.A., 2008.
[11] R. Ghosh, G.A. Buxton, O.B. Usta, A.C. Balazs, A. Alexeev, Langmuir, 26 (2010) 2963-2968.
[12] M. Hill, N. Harris, Ultrasonic Particle Manipulation, in: S. Hardt, F. Schönfeld (Eds.) Microfluidic Technologies for Miniaturized Analysis Systems, Springer US, 2007, pp. 357-392.
[13] M. Hill, N.R. Harris, Ultrasonic Microsystems for Bacterial Cell Manipulation, in: M. Zourob, S. Elwary, A. Turner (Eds.) Principles of Bacterial Detection: Biosensors, Recognition Receptors and Microsystems, Springer New York, 2008, pp. 909-928.
[14] J. Branscomb, A. Alexeev, Soft Matter, 6 (2010) 4066-4069.
[15] H. Masoud, A. Alexeev, Soft Matter, 7 (2011) 8702-8708.
[16] H. Masoud, A. Alexeev, Chem. Commun., 47 (2011) 472-474.
[17] S. Succi, The lattice Boltzmann equation for fluid dynamics and beyond, Oxford University Press, Oxford, 2001.
[18] A.J.C. Ladd, R. Verberg, J. Stat. Phys., 104 (2001) 1191-1251.
[19] G.A. Buxton, C.M. Care, D.J. Cleaver, Model. Simul. Mater. Sc., 9 (2001) 485-497.
[20] A.J.C. Ladd, J.H. Kinney, T.M. Breunig, Phys. Rev. E, 55 (1997) 3271-3275.
[21] A. Alexeev, R. Verberg, A.C. Balazs, Langmuir, 23 (2007) 983-987.
[22] A. Alexeev, R. Verberg, A.C. Balazs, Macromolecules, 38 (2005) 10244-10260.
[23] A. Alexeev, R. Verberg, A.C. Balazs, Phys. Rev. Lett., 96 (2006) 148103.
[24] M. Bouzidi, M. Firdaouss, P. Lallemand, Phys. Fluids, 13 (2001) 3452-3459.
[25] G.D. Zhu, A. Alexeev, E. Kumacheva, A.C. Balazs, J. Chem. Phys., 127 (2007) 034703.
[26] W. Mao, A. Alexeev, Phys. Fluids, 23 (2011) 051704.
[27] J.P. Arata, A. Alexeev, Soft Matter, 5 (2009) 2721-2724.
[28] K.A. Smith, A. Alexeev, R. Verberg, A.C. Balazs, Langmuir, 22 (2006) 6739-6742.
[29] A. Kilimnik, W. Mao, A. Alexeev, Phys. Fluids, (2011) in press.
[30] P. Vasseur, R.G. Cox, J. Fluid Mech., 80 (1977) 561-591.
[31] R.G. Cox, J. Fluid Mech., 44 (1970) 791-810.
[32] W.H. Grover, A.K. Bryan, M. Diez-Silva, S. Suresh, J.M. Higgins, S.R. Manalis, P. Natl. Acad. Sci. USA, (2011).
[33] B.A. Evans, A.R. Shields, R.L. Carroll, S. Washburn, M.R. Falvo, R. Superfine, Nano Lett, 7 (2007) 1428-1434.

[34] J. den Toonder, F. Bos, D. Broer, L. Filippini, M. Gillies, J. de Goede, T. Mol, M. Reijme, W. Talen, H. Wilderbeek, V. Khatavkar, P. Anderson, Lab Chip, 8 (2008) 533-541.
[35] K. Oh, J.H. Chung, S. Devasia, J.J. Riley, Lab Chip, 9 (2009) 1561-1566.
[36] B. Pokroy, A.K. Epstein, M.C.M. Persson-Gulda, J. Aizenberg, Adv. Mater., 21 (2009) 463-469.
[37] M.K. Kwak, H.E. Jeong, T.I. Kim, H. Yoon, K.Y. Suh, Soft Matter, 6 (2010) 1849-1857.
[38] N.A. Malvadkar, M.J. Hancock, K. Sekeroglu, W.J. Dressick, M.C. Demirel, Nature Mater., 9 (2010) 1023-1028.

Figure captions

Figure 1 (color online). Schematic of computational setup.

Figure 2 (color online). Particle trajectories for particles with different dimensionless external forces W in posted microchannels and in a microchannel with smooth walls. Particle radius is $R = 0.25L$ and it is initially located at $y = 0.167L_y$ and $z = 0$.

Figure 3 (color online). Period-averaged cross-stream velocity (a) in a microchannel with posts normal to the bottom wall, and (b) in a microchannel with posts tilted 45 degrees against the flow direction. The dotted lines show the contours of surface posts. The arrows show the magnitude and direction of averaged flow velocity. The colors (grayscale) indicate the magnitude of the dimensionless flow vorticity.

Figure 4. Equilibrium positions of particles with $R = 0.25L$ and $W = 8.37$ in a channel with posts tilted 45 degrees against the flow direction. The equilibrium positions are calculated by averaging particle trajectories over on structure period in the x direction. The dotted lines show the location of surface posts.

Figure 5 (color online). Cross-stream trajectories of particles with different W. Particle radius is $R = 0.25L$.

Figure 6. Dimensionless critical force W_{cr} as a function of particle radius R in channels with posted and smooth walls. The inset shows the ratio between critical forces in posted and smooth channels.

Figure 7. Equilibrium positions of particles with $R = 0.25L$ in channels with posts with different tilt angle α.

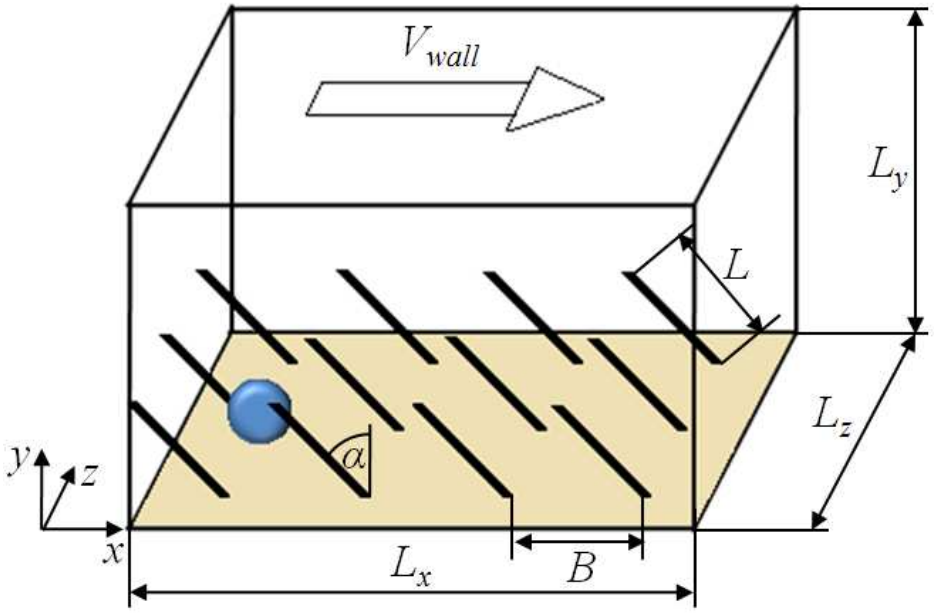

Figure 1

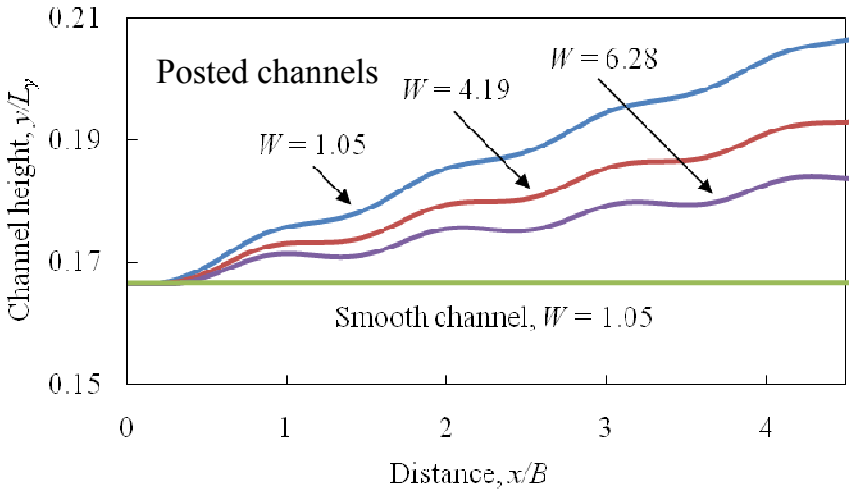
0.21
0.19
0.17
0.15
Channel height, y/L_y
Posted channels
$W = 6.28$
$W = 4.19$
$W = 1.05$
Smooth channel, $W = 1.05$
0
1
2
3
4
Distance, x/B

Figure 2

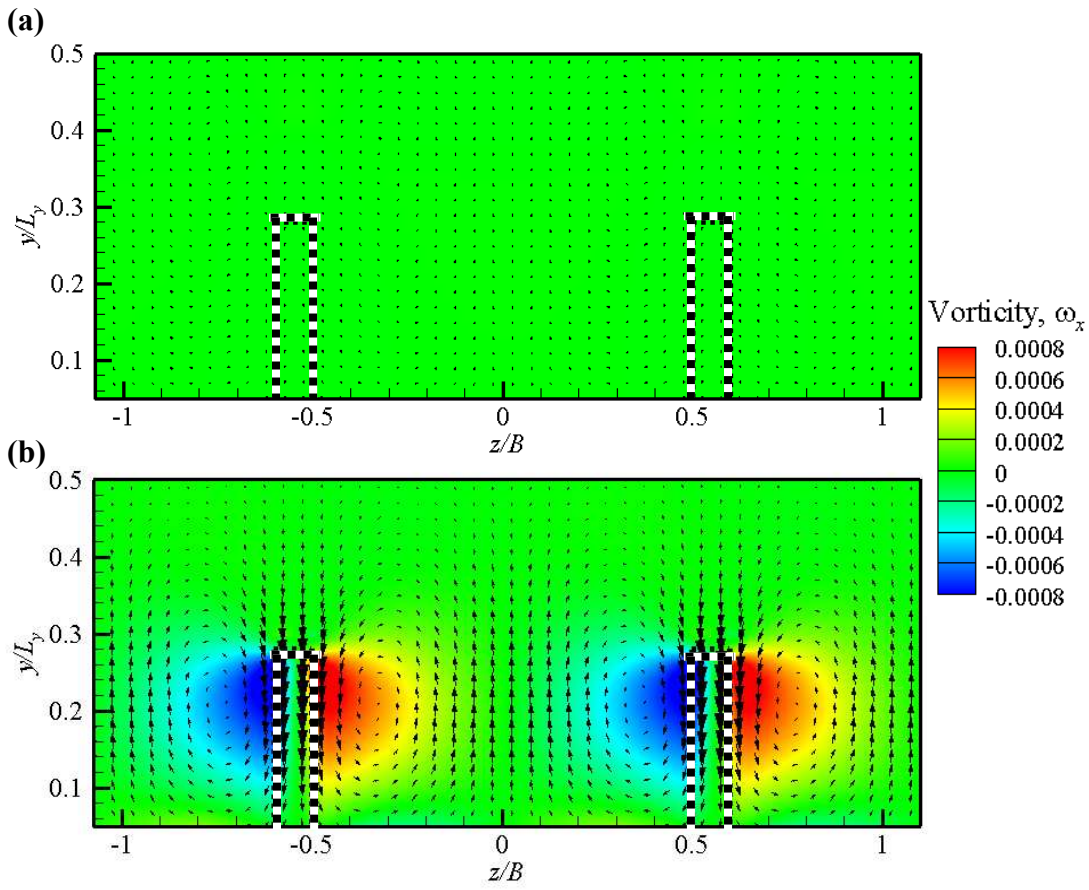
(a)
(b)
0.5
0.4
0.3
0.2
0.1
y/L_y
-1
-0.5
0
0.5
1
z/B
Vorticity, ω_x
0.0008
0.0006
0.0004
0.0002
0
-0.0002
-0.0004
-0.0006
-0.0008

Figure 3

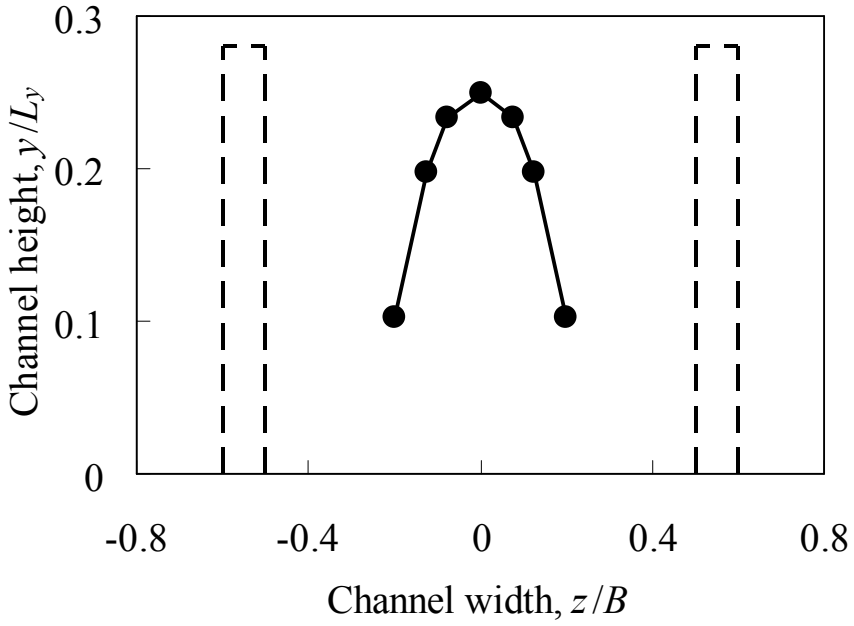

Figure 4

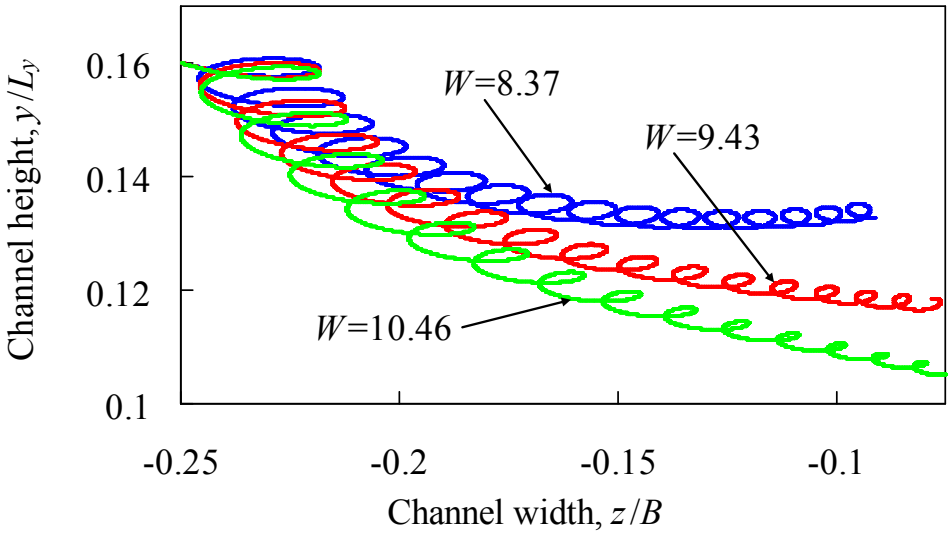
0.16
0.14
0.12
0.1
Channel height, y/L_y
W=8.37
W=9.43
W=10.46
-0.25
-0.2
-0.15
-0.1
Channel width, z/B

Figure 5

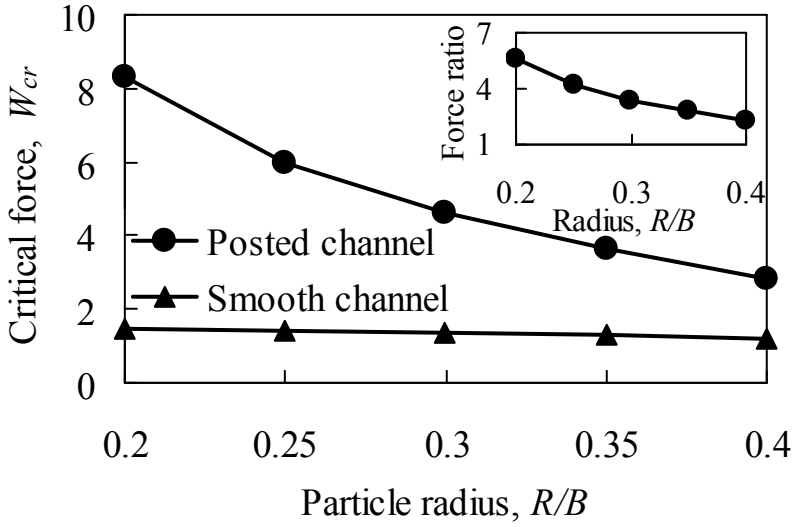
Critical force, W_{cr}
10
8
6
4
2
0
0.2
0.25
0.3
0.35
0.4
Particle radius, R/B
Posted channel
Smooth channel
Force ratio
7
4
1
0.2
0.3
0.4
Radius, R/B

Figure 6

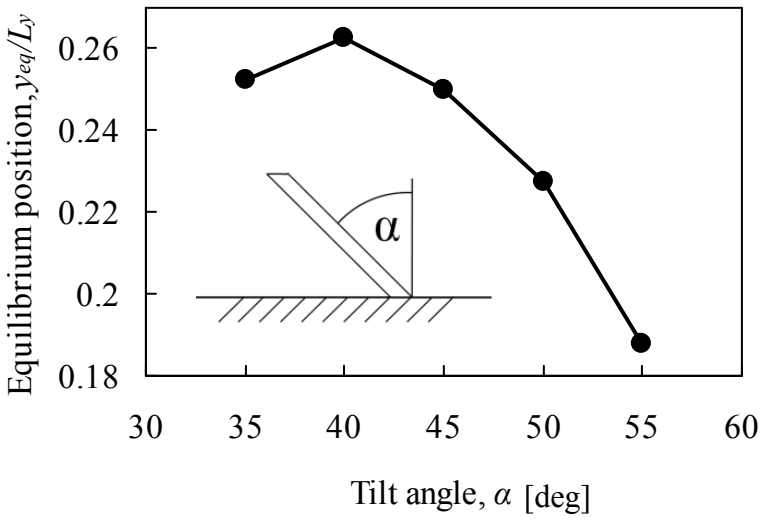
Equilibrium position, y_{eq}/L_y
0.26
0.24
0.22
0.2
0.18
30
35
40
45
50
55
60
α
Tilt angle, α [deg]

Figure 7